Journal of Physics: Conference Series **2767** (2024) 052045 doi:10.1088/1742-6596/2767/5/052045

Numerical simulation of stabilisation of floating wind with submerged hydrofoil

Junxian Wang[1], Liang Yang[1,2], Jingru Xing[1], Jianhui Yang[2]

[1] Division of Energy and Sustainability, School of Water, Energy and Environment (SWEE), Cranfield University, Bedford, MK43 0AL, UK
[2] Voxshell Ltd, Cranfield, Bedford, MK43 0FQ, UK

E-mail: liang.yang@cranfield.ac.uk

Abstract. This research focuses on the optimal design and method of attaching a submerged hydrofoil to an offshore platform to enhance stabilisation. The flapping hydrofoil, exhibiting a hybrid motion combining heave and pitch, is engineered to convert incoming wave energy. It generates a distinctive wake that effectively counteracts incoming waves, thereby reducing wave impact. In this study, a NACA0030-type hydrofoil was strategically positioned between two columns of the platform model. Comprehensive analyses were conducted to evaluate the free-floating platform's response to regular waves, with a focus on the attached hydrofoil. The results indicate that the hydrofoil significantly reduces the surge motion and drifting speed of the platform, affirming its effectiveness in enhancing stabilisation.

1. Introduction

To address the global consequences and challenges posed by climate change—such as the need to reduce greenhouse gas emissions and decrease reliance on non-renewable energy sources—floating offshore wind turbines have captured the interest of both industry and academia due to their excellent performance in deep-water environments. While the addition of a mooring line system can stabilise the foundation, the high commercial cost of such lines cannot be overlooked. Consequently, there's a pressing need to enhance the stabilisation of the floating foundation and minimise of mooring line loads.

The concept of a foil-shaped structure, deriving inspiration from the natural mechanisms of birds and fish, has been identified as capable of generating forward thrust through its flapping behaviour [1]. When submerged, a hydrofoil can exhibit both heaving and pitching responses under wave conditions [2, 3]. This leads to the creation of a jet-like wake, wherein the hydrofoil experiences thrust due to the higher velocity of flow in the wake compared to the ambient or oncoming flow. Such a phenomenon allows the hydrofoil to transform wave-induced kinetic energy into propulsive force, effectively enabling movement against the direction of wave motion [4], termed as Wave Devouring Propulsion (WDP) [5]. Foil attachment to ship hull could generate green thrust in waves, significantly reducing fuel costs [6]. However, the incorporation of WDP technology into offshore platforms is still an emerging field [7], offering fertile ground for future research and innovation in marine propulsion systems.

Numerical investigations on flapping hydrofoils typically involve both potential theory and Computational Fluid Dynamics (CFD). For potential flow solvers, Boundary Element Methods (BEM) are widely used to simulate actively controlled hydrofoils, where the flap motion is

Content from this work may be used under the terms of the Creative Commons Attribution 4.0 licence. Any further distribution of this work must maintain attribution to the author(s) and the title of the work, journal citation and DOI.
Published under licence by IOP Publishing Ltd

predetermined [8, 9, 10]. Notably, Belibassakis and Politis [10] studied flapping hydrofoils in wave conditions to enhance ship propulsion and found significant thrust production due to hydrofoils, accounting for 10% to 50% of a ship's calm-water resistance at equivalent speeds. The system notably improved the ship's propulsive performance and dynamic stabilisation, providing a rationale for adopting horizontal hydrofoil configurations in this study. For its investigation via CFD, De Silva and Yamaguchi [11] numerically explored active 2D oscillation hydrofoils in wavy flows and suggested that over 50% of wave energy could be converted into propulsion energy when the wave amplitude to hydrofoil chord ratio ranged from 1/14 to 3/14. Liu et al. [12] examined 2D rigid and flexible flapping hydrofoils in regular waves and found enhanced performance when the hydrofoil's frequency matched the wave frequency, which was confirmed by Xu et al. [9]. In addition to examining the wave-propelled physical mechanisms of hydrofoils, numerical studies have also focused on their impact on ship propulsion. By employing potential theory (AQWA) and CFD (Fluent), Wang et al. [13] analysed the motion of a 3D low-speed wave-powered unmanned catamaran ship with and without horizontally fixed hydrofoils under head waves, and found thrust generation via the attached hydrofoils, as well as the mitigation of ship's heave, pitch, wave-added resistance.

The present paper numerically studies the dynamic response of a free-floating platform equipped with a submerged hydrofoil in regular waves using OpenFOAM, an open-source CFD software. The results indicate that attaching a hydrofoil can significantly enhance the stabilisation of the floating platform. Specifically, surge motion and the drift speed are substantially suppressed. The findings of this study could offer valuable insights and serve as a reference for the design and operation of moored floating platforms. The paper is organised as follows: Section 2 provides a detailed description of the numerical arrangement, detailing the computational domain and boundary condition, as well as the obtained mesh strategy. Section 3 discusses the convergence test of two-dimensional numerical wave tank (NWT) and three-dimensional wave floater interaction (WFI). Section 4 investigates the impact of the attached foil on the offshore platform's dynamic response in waves. Finally, Section 5 summarises the conclusions of the study.

2. Numerical configurations

The present study utilised the open-source CFD simulation software, OpenFOAM-v2106 and v2206, along with the meshing software ChopMesh [14], to perform numerical simulations. The interFoam-based solver within OpenFOAM was employed to solve the Navier-Stokes equations and the associated 6 degrees of freedom (DoF) motion equations. Regular waves were generated using an in-built utility in OpenFOAM by directly specifying wave parameters at the inlet boundary. Fluid in the simulations was characterised by the incompressible Reynolds-averaged Navier-Stokes equations. The k-omega SST (Shear Stress Transport) turbulence model was applied. The volume of fluid (VOF) method was adopted to identify the air-water interface, defining a volume fraction of water as α_1.

The target floater of the present study is exhibited in Figure 1a, which includes a typical floating platform and an fixed hydrofoil model. The floating platform model was set up based on the well-known OC6 (Offshore Code Comparison Collaboration, Continued with Correlation and unCertainty) project [15, 16], OC5 project [17], and its parameters can be found in Robertson et al. [17]. The hydrofoil model selected is of the NACA0030 type and is horizontally assembled in the gap between two columns, as indicated by the blue colour in Figure 1a. The illustration of this foil model is provided in Figure 1b, where the chord length (c) is the distance between the hydrofoil's leading edge and trailing edge, and the span length (d) denotes hydrofoil's transverse distance. A scale factor λ of 100 was applied to this study and parameters of the hydrofoil model are given in Table 1. The pivot (P) of the hydrofoil is co-axial with the horizontal rod of the floating platform, and the definition of pivot ratio is the distance ratio of its location to

leading edge (AP) and trailing edge (PB). The foil model was submerged to a depth of 0.23 m (i.e., draft). A simplification for this numerical study should be noted that the attachment of hydrofoil doesn't affect the original floater's mass and moment of inertia.

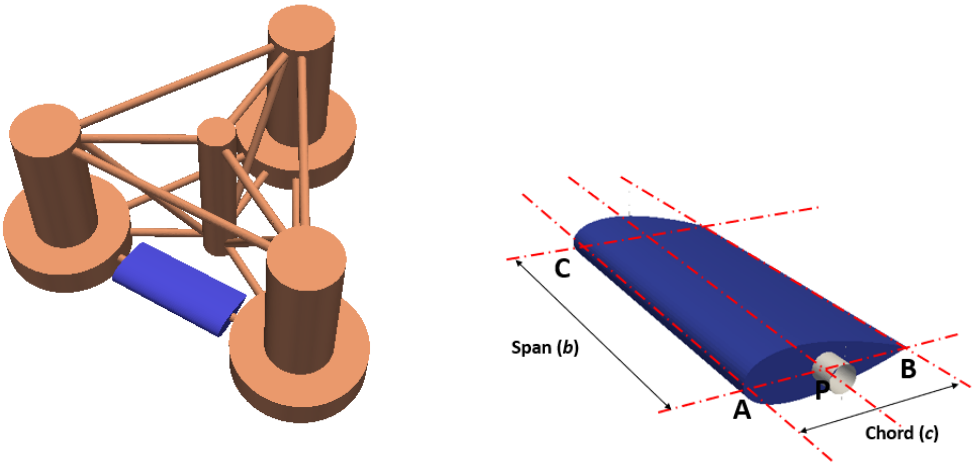

(a) (b)

Figure 1: Three-dimensional model of the floating platform attached with a fixed hydrofoil (a) and the illustration of hydrofoil model (b).

Table 1: Parameters of the hydrofoil model.

Parameters	Chord c	Span d	Pivot ratio	Draft
Values	0.1 m	0.23 m	0.9	0.23 m

Figure 2 illustrates the side-view of the computational domain layout. The entire numerical wave tank (NWT) is 20 m long, 2.5 m high, 2 m wide, with a water depth of 1.5 m. The wavemaker is specified at X = 0 m, generating the wave along the X-direction. The floater is positioned at 5.25m downstream, approximately 1.5 times the wavelength. The grey area marked in Figure 2 is used to reduce wave reflection. As this simulation employs "Overset" mesh technique to achieve the floater's dynamic response in waves, the mesh strategy is specified in two regions. The outer region, known as the background mesh, is created by OpenFOAM's in-built mesh generator and is presented in Figure 3. The Cartesian mesh is used and a 2-level mesh refinement is implemented towards the water surface. In the far end of the background mesh, which is the wave absorption area coloured in grey in Figure 2, the mesh size along the X-direction is given an expansion to weaken wave propagation and further mitigate the impact of wave reflection. In this method, the mesh expansion ratio and the end cell's size play a crucial role in reducing wave reflection.

Located in a small area surrounding the floater, the inner region mesh is generated using ChopMesh [14] and is presented in Figure 4. In contrast to typical inner region shapes, such as a cylinder or a cube, the outline of the current inner region mesh in Figure 4a is inflated based

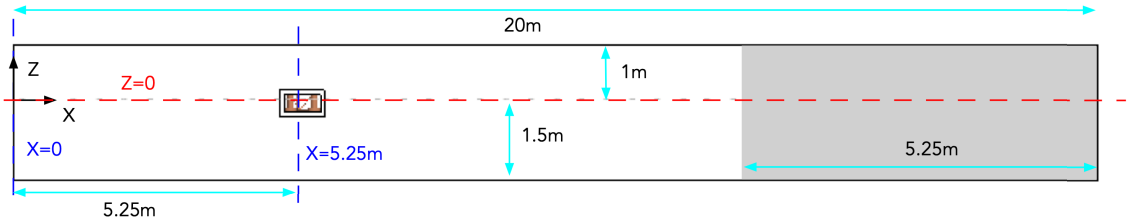

Figure 2: Description of the computational domain.

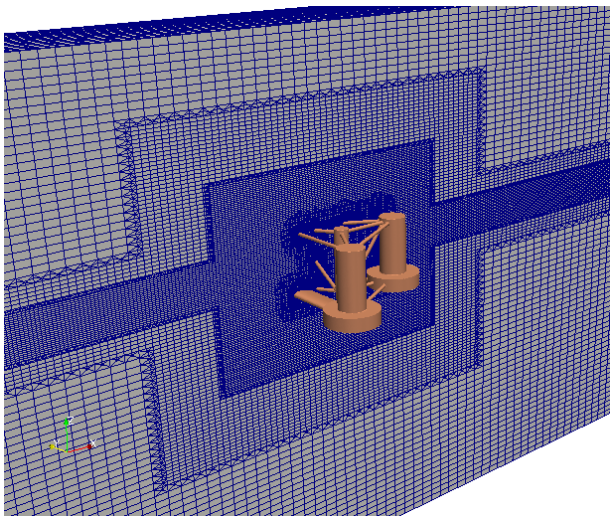

Figure 3: Mesh arrangement of the computational domain.

on the floater's geometry, effectively reducing the mesh cell number. A close-up view to inspect mesh details is provided in Figure 4b. The hexahedral-dominant mesh exhibits good quality, particularly in terms of perfect geometry fitting, especially along the edges, such as the trailing edges (Figure 4b). The inner region mesh undergoes three levels of refinement.

3. Convergence test

This numerical study prepared and applied a total of 7 sets of meshes, and corresponding details are summarised in Table 2. All cases shares the identical regular wave (0.14 m wave height, 1.5 s wave period) scaled down from the wave in Greater Ekofisk area [18]. Case 1 to 6 are used for the two-stage convergence test. For stage 1, Cases 1 to 3 correspond to the coarse mesh, medium mesh, and fine mesh, respectively, and were used to generate the target wave in the two-dimensional (2D) numerical wave tank (NWT). Subsequently, stage 2 carried out the wave-floater interaction (WFI) simulation in a three-dimensional (3D) wave tank, using three sets of meshes: coarse for Case 4, medium for Case 5 and fine for Case 6. Meshes of the 3D wave tank share identical X-Z planar mesh density with that of the 2D NWT. For the WFI

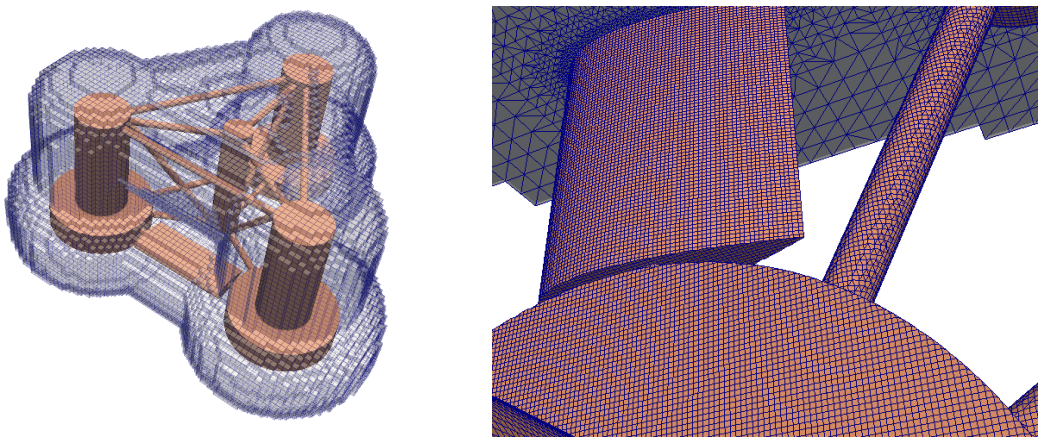

(a) (b)

Figure 4: Mesh arrangement of near the floater (a) and close-up the floater (b).

simulation, the reference cell of the inner region mesh is cubic (i.e., the identical size (d_{ref}) at X, Y, Z directions) and its size depends on the mesh resolution near the water surface. The aspect ratio (i.e., d_x/d_z) of mesh size near the water surface varies for coarse mesh and medium/fine mesh. As a result, the reference cell size (d_{ref}) of inner region was determined as the average of d_x and d_z of the mesh size near the water surface.

Table 2: Mesh setting summary of all included cases.

Case	Label	Mesh	d_{ref}	Cell number	Description
1	M1-2D-NWT	coarse		3.0e+4	
2	M2-2D-NWT	medium		4.4e+4	
3	M3-2D-NWT	fine		5.5e+4	
4	M1-3D-WFI	coarse	0.0175m	3.7e+6	platform only
5	M2-3D-WFI	medium	0.0131m	6.9e+6	platform only
6	M3-3D-WFI	fine	0.0117m	9.0e+6	platform only
7	M4-3D-WFI	fine	0.0117m	9.2e+6	platform + foil

The collected wave data at X = 5.25 m from Case 1 to 3 are shown in Figure 5, including the time series of wave elevation and corresponding wave spectra. For better comparison, the involved time series were slightly shifted to ensure their symmetrical distribution on both side of zero wave elevation in Figure 5a. It could be observed that the wave elevation changing against time shows consistency among Case 1 to 3, especially that from Case 2 (medium) and Case 3 (fine). A complete 10 peak-to-peak wave-changing cycles were selected to calculate the wave spectra and displayed in Figure 5b. The three Cases (1 to 3) share identical wave frequency. The wave amplitudes in Figure 5b indicates reliable results from medium and fine mesh. Subsequently, the heave motion of the floater from Case 4 to 6 is obtained from the vertical displacement of the floater's Centre of Gravity (CoG) and presented in Figure 6. Similarly, for better comparison, it should be noted that curves in Figure 6a are shifted upwards, symmetrical

to 0, as well as heave comparison of with/without the hydrofoil in Figure 8a. Time series of the heave motion in Figure 6a are in great agreement with each other. The averaged value of four peaks in Figure 6a is extracted to give a quantitative analysis and summarised in Figure 6b. The values of Case 5 and 6 remain constant, suggesting the acceptable simulations using medium and fine mesh.

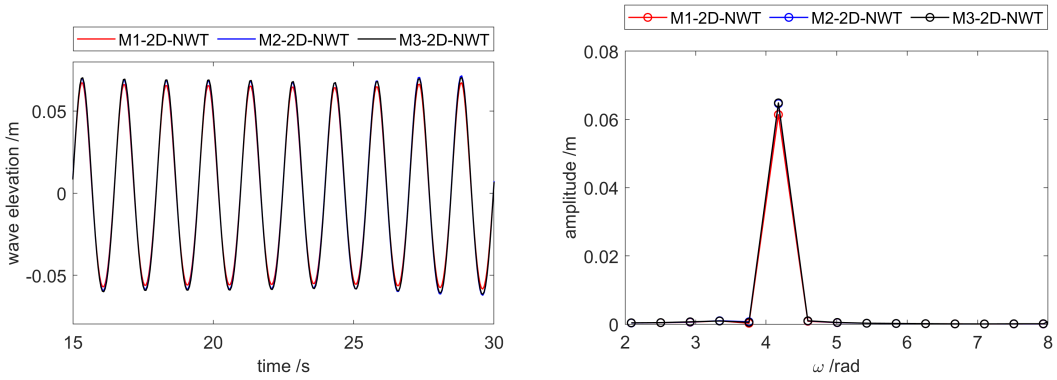

(a) (b)

Figure 5: Convergence test results of the 2D numerical wave tank (NWT): wave time history (a) and wave spectra (b) at X = 5.25 m.

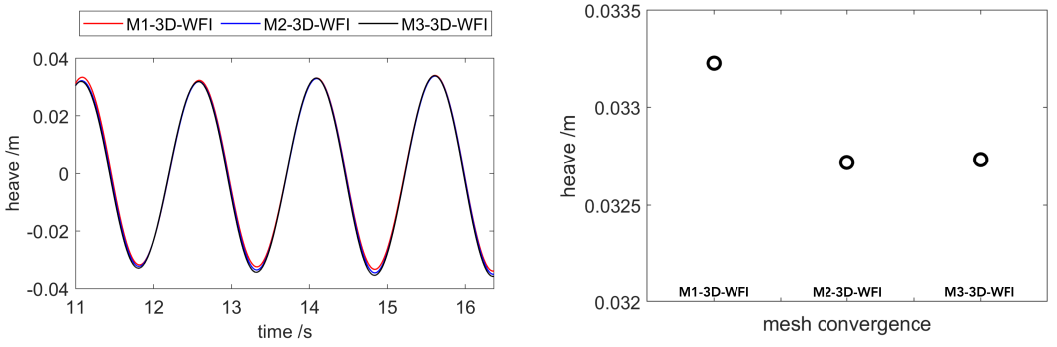

(a) (b)

Figure 6: Convergence test results of the heave motion of platform only: time history (a) and averaged peak (b).

4. Results and discussion

The free-floating platform with the fixed hydrofoil was then simulated under the identical wave using the fine mesh, namely Case 7 in Table 2. An animation snapshot, depicted in Figure 7, shows the interaction between the floating platform and the hydrofoil with the oncoming wave. The comparison of Case 6 and Case 7 is discussed in this section, including the floater's heave motion and surge motion, to reveal the impact of the hydrofoil. A potential explanation for the observed difference is then provided by associating it with the flow field analysis near the hydrofoil. The heave and surge response of the free-floating floater in a regular wave (0.14 m wave height, 1.5 s wave period) from Case 6 and Case 7 are studied and shown in Figure 8 to reveal the impact of hydrofoil.

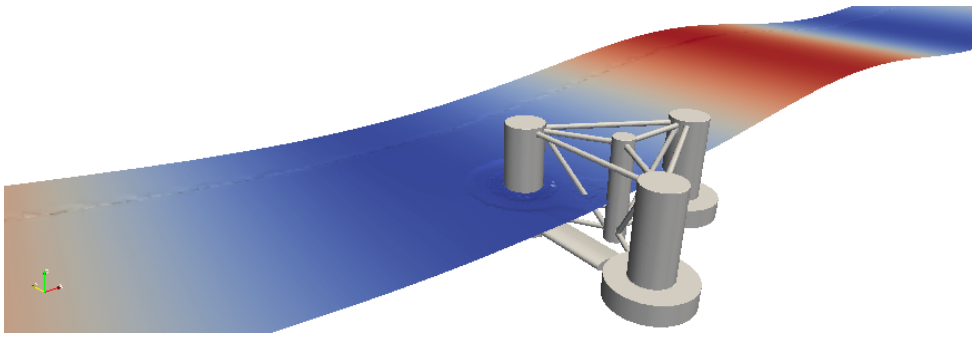

Figure 7: An animation capture of the platform with hydrofoil (b) at $t = 16$ s.

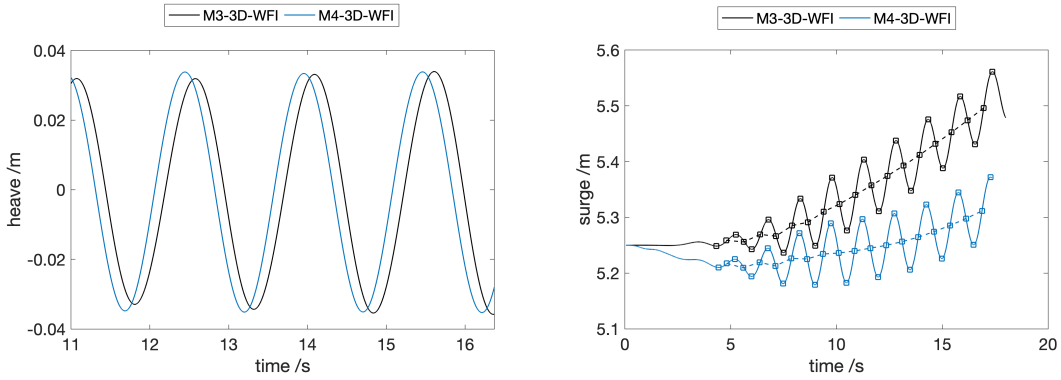

(a) (b)

Figure 8: Results of the heave motion (a) and the surge motion (b) of platform only and platform with foil.

The heave curves from M3-3D-WFI and M4-3D-WFI in Figure 8a share the similar trend with similar upper and lower limit, but slightly differ in phase. The comparison of surge curves for the free-floating state in Figure 8b demonstrates that the drift speed of the platform with a hydrofoil (M4-3D-WFI) is significantly suppressed. This is highlighted by two lines of fit obtained based on the local maxima/minima of surge motion. This suggests that the inclusion of a hydrofoil leads to a reduction in the horizontal drifting force. Studies has prove that the different patterns of vortex shedding [19] after the flapping hydrofoil give rise to the drag-thrust transition. The instantaneous ($t = 16$ s)velocity vector field near the hydrofoil is plotted and shown in Figure 9, where a distinct vortex is observed near the hydrofoil's trailing edge, as marked within the red dash square. The attached hydrofoil rotates with the point out of its geometry, resulting in a motion different from that of a normal flapping foil [20]. Consequently, the vortex in Figure 9 appears near the sharp edge, with surrounding flow vectors pointing towards the thicker side. This generated vortex is speculated to account for the reduction in the floater's drifting speed.

5. Conclusion

A submerged hydrofoil can make flapping motion in response to wave excitation, achieving the conversion of wave energy to green thrust. This technology holds huge potential to assist traditional ship propulsion systems. The present study attempted to fix a submerged hydrofoil to a floating offshore platform and conducted numerical simulations to investigate the heave and surge motion of a free-floating floater in regular waves, focusing on the hydrofoil's effect.

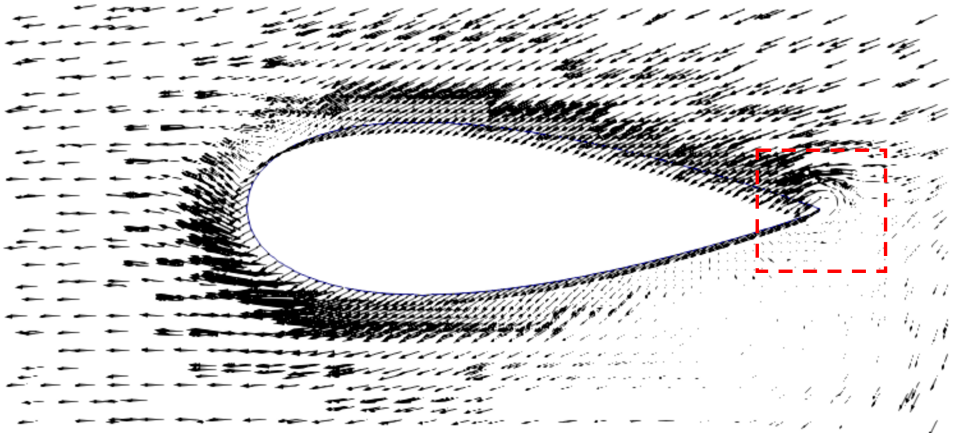

Figure 9: Velocity vector field near the foil at $t = 16$ s.

Corresponding results demonstrate that attaching a hydrofoil to the free-floating platform significantly reduces both the platform's drift speed and drifting force. Additionally, for the moored floating platform, it is inferred that mooring loads are reduced due to the hydrofoil attachment mitigating drifting force, thus providing valuable reference for design optimisation.

Acknowledgements

L. Yang acknowledges the support from Higher Education Innovation Funding (HEIF) from Cranfield University and GFIL Future Frontiers Fund, 'Novel Floating Wind Platform'.

References

[1] Xia Wu, Xiantao Zhang, Xinliang Tian, Xin Li, and Wenyue Lu. A review on fluid dynamics of flapping foils. *Ocean Engineering*, 195:106712, 2020.

[2] Jingru Xing, Dimitris Stagonas, Phil Hart, Chengchun Zhang, Jianhui Yang, and Liang Yang. Wave induced thrust on a submerged hydrofoil: pitch stiffness effects. *arXiv preprint arXiv:2209.05551*, 2022.

[3] Junxian Wang, Sabin Santhosh, Oriol Colomés, Matteo Capaldo, and Liang Yang. Experimental study of dynamic response of passive flapping hydrofoil in regular wave. *Physics of Fluids*, 35(7), 2023.

[4] Jingru Xing and Liang Yang. Wave devouring propulsion: An overview of flapping foil propulsion technology. *Renewable and Sustainable Energy Reviews*, 184:113589, 2023.

[5] Yutaka Terao. Wave devouring propulsion system: From concept to trans-pacific voyage. In *International Conference on Offshore Mechanics and Arctic Engineering*, volume 43444, pages 119–126, 2009.

[6] James Andrew Bowker and NC Townsend. Evaluation of bow foils on ship delivered power in waves using model tests. *Applied Ocean Research*, 123:103148, 2022.

[7] L Yang, A Koutras, F Topal, A Kolios, and D Stagonas. Working with nature: retrofitting solutions for reducing mooring line loads.

[8] ES Filippas and KA Belibassakis. Hydrodynamic analysis of flapping-foil thrusters operating beneath the free surface and in waves. *Engineering Analysis with Boundary Elements*, 41:47–59, 2014.

[9] GD Xu, WY Duan, and BZ Zhou. Propulsion of an active flapping foil in heading waves of deep water. *Engineering Analysis with Boundary Elements*, 84:63–76, 2017.

[10] Kostas A Belibassakis and Gerasimos K Politis. Hydrodynamic performance of flapping wings for augmenting ship propulsion in waves. *Ocean Engineering*, 72:227–240, 2013.

[11] Liyanarachchi Waruna Arampath De Silva and Hajime Yamaguchi. Numerical study on active wave devouring propulsion. *Journal of marine science and technology*, 17(3):261–275, 2012.

[12] Peng Liu, Yebao Liu, Shuling Huang, Jianfeng Zhao, and Yumin Su. Effects of regular waves on propulsion performance of flexible flapping foil. *Applied Sciences*, 8(6):934, 2018.

[13] Dongjiao Wang, Kun Liu, Ping Huo, Shouqiang Qiu, Jiawei Ye, and Fulin Liang. Motions of an unmanned catamaran ship with fixed tandem hydrofoils in regular head waves. *Journal of Marine Science and Technology*, 24(3):705–719, 2019.

[14] Voxshell Limited. Mesh generation method. *GB2311129.7*, 2023.

[15] Amu N Robertson, Sébastien Gueydon, Erin Bachynski, Lu Wang, Jason Jonkman, Daniel Alarcon, Ervin Amet, Alec Beardsell, Paul Bonnet, Bastien Boudet, et al. Oc6 phase i: Investigating the underprediction of low-frequency hydrodynamic loads and responses of a floating wind turbine. In *Journal of Physics: Conference Series*, volume 1618, page 032033. IOP Publishing, 2020.

[16] Lu Wang, Amy Robertson, Jason Jonkman, Jang Kim, Zhi-Rong Shen, Arjen Koop, Adrià Borràs Nadal, Wei Shi, Xinmeng Zeng, Edward Ransley, et al. Oc6 phase ia: Cfd simulations of the free-decay motion of the deepcwind semisubmersible. *Energies*, 15(1):389, 2022.

[17] Amy N Robertson, Fabian Wendt, Jason M Jonkman, Wojciech Popko, Habib Dagher, Sebastien Gueydon, Jacob Qvist, Felipe Vittori, José Azcona, Emre Uzunoglu, et al. Oc5 project phase ii: validation of global loads of the deepcwind floating semisubmersible wind turbine. *Energy Procedia*, 137:38–57, 2017.

[18] DNV GL-OS-E301. Offshore standard - position mooring (dnvgl-os- e301). *Edition July 2017*, 2017.

[19] NS Lagopoulos, GD Weymouth, and Bharathram Ganapathisubramani. Universal scaling law for drag-to-thrust wake transition in flapping foils. *Journal of Fluid Mechanics*, 872:R1, 2019.

[20] ChunYin Chan, Junxian Wang, Liang Yang, and Jun Zang. Wave-assisted propulsion: An experimental study on traveling ships. *Physics of Fluids*, 36(2), 2024.

https://dspace.org/

Numerical simulation of stabilisation of floating wind with submerged hydrofoil

Wang, Junxian; Yang, Liang; Xing, Jingru; Yang, Jianhui

2024-06-10
IOP Publishing
https://doi.org/10.1088/1742-6596/2767/5/052045
Wang J, Yang L, Xing J, Yang J. (2024) Numerical simulation of stabilisation of floating wind with submerged hydrofoil. In: Journal of Physics: Conference Series, Volume 2767, Issue 5, June 2024, Article number 052045

Downloaded from a DSpace repository. https://dspace.org/